Published in final edited form as:
New J Phys. 2009 October 1; 11: 105046. doi:10.1088/1367-2630/11/10/105046.

Mode selectivity with polarization shaping in the mid-IR

David B Strasfeld, **Chris T Middleton**, and **Martin T Zanni**
Department of Chemistry, University of Wisconsin-Madison, 1101 University Avenue, Madison, WI 53706-1396, USA, zanni@chem.wisc.edu

Abstract

We report that polarization-shaped mid-infrared (IR) pulses can be used to enhance the vibrational population of one mode over another in a coupled molecular system. A genetic algorithm and a new mid-IR polarization shaper were used to alter the relative vibrational excitation of the two carbonyl stretching modes in $Mn(CO)_5Br$. One mode could be selectively enhanced over the other by 2–3 times. Control over the polarization leads to better optimization than phase-only control. Several possible mechanisms that indicate how polarization shaping leads to selective vibrational excitation are discussed using a formalism that separates polarization shaping effects on the signal strength from amplitude or phase shaping. The techniques introduced herein will have broad applications in quantum gating schemes, controlling ground state chemistry and enhancing the sensitivity of multidimensional IR and visible spectroscopies.

1. Introduction

Polarization is a commonly used tool in femtosecond spectroscopies. It is particularly important in two-dimensional infrared (2D IR) and optical (2D Vis) spectroscopies where polarized pulse sequences can be used to measure the angles between transition dipoles [1]–[3], study the rotational motions of molecules, enhance cross peaks or eliminate diagonal peaks [4], and suppress background signals [2,5]. 2D spectroscopies are at least 3rd-order techniques, so that there are a minimum of four electric field interactions between the sample and the incident and emitted electric fields, each of which can be manipulated. 3D spectroscopies [6,7] have at least two additional polarization variables. Polarization has long been used as a spectroscopic tool, but it is especially useful in multidimensional spectroscopies because the diagonal and cross peaks that appear in 2D and 3D spectra arise from a well-defined number and ordering of the pulsed electric fields with the molecular transition dipoles.

Control over polarization generally leads to improved spectral resolution by enhancing or suppressing peaks in 2D IR spectra [4]. This paper investigates whether the 2D IR spectral resolution can be further enhanced by pairing polarization control [8]–[12] with the signal optimization achieved by a genetic learning algorithm [13]. Genetic learning algorithms and feedback loops are powerful means of manipulating both ground and excited state vibrational motions as well as controlling chemical reactions [14]–[22]. Most of the work in coherent control and pulse shaping has been done using near-IR, visible or UV laser light. A few years ago, our research group extended some of these methods into the mid-IR by developing a Ge acousto-optic modulator that is capable of modulating the phase and amplitude of mid-IR pulses [23,24]. Using this shaper, we demonstrated that it was possible to control vibrational excitations in the antisymmetric stretch mode of $W(CO)_6$ [25,26]. Chirped mid-IR pulses have long been known to cause high vibrational excitation via ladder climbing [27] or using shaped Raman pulses [28,29]. With mid-IR pulse shaping, we could equalize or even invert the

Correspondence to: Martin T Zanni.

populations of excited vibrational levels. Similar manipulations are frequently used in NMR spectroscopy to increase signal strength or remove unwanted spin resonances.

Recently, we extended our pulse shaping methodology to control over the phase, amplitude and polarization of the mid-IR pulses [30]. Our technique for polarization control is based on the work by Plewicki *et al*, who demonstrated a simple method for polarization shaping in which the vertical and horizontal electric fields are shaped on two halves of the same liquid crystal modulator before being recombined into a single collinearly propagating beam [9]. Such an approach is particularly well suited for implementation in shapers like ours, which use an AOM. With this approach, we now have complete control over the electric field characteristics and can programme nearly arbitrary pulse sequences [30]. In this paper, we demonstrate that the population of either one of two strongly coupled vibrational modes in $Mn(CO)_5Br$ can be enhanced over the other with polarization-tailored mid-IR pulses and that polarization shaping leads to improved enhancement over phase shaping alone. The enhancement of 2D IR spectra with polarization shaping has been predicted previously in simulations of the pump–probe spectra of a helical pentamer [31]. Polarization shaping in the visible region of the spectrum has been used to optimize yields in the multiphoton ionizations of K_2 [32] and NaK [33]. To understand the process by which polarization shaping alters the signal intensity, we present a formalism that separates the orientational molecular response from the vibrational molecular response so that polarization shaping can be calculated independently of amplitude and phase shaping. Our experimental observations and theoretical predictions have potentially important consequences for improving the sensitivity of multidimensional IR spectroscopies and other fields utilizing quantum control.

2. Experimental

We set out to alter the contributions of the doubly degenerate E and nondegenerate A_1 modes of $Mn(CO)_5Br$ to the pump–probe spectrum relative to one another. $Mn(CO)_5Br$ exhibits C_{4v} symmetry and a slightly distorted octahedral geometry. The axial A_1 mode is primarily localized on the carbonyl opposite the Br atom and gives rise to a feature at 2002 cm^{-1}. The E mode is localized on the four equatorial carbonyls, is doubly degenerate and gives rise to a more intense feature at 2052 cm^{-1}. For our experiments, $Mn(CO)_5Br$ was dissolved in *n*-hexane and placed between two CaF_2 plates separated by a 75 μm thick Teflon spacer to yield an OD of 0.7. Sample degradation was accounted for by observing changes in the transform-limited pump–probe spectrum before and after each optimization, which were negligible.

2.1. Polarization shaping

The optical layout used for our experiments is diagrammed in figure 1 and is described in detail elsewhere [30]. Difference frequency mixing of the signal and idler outputs of a β-barium borate (BBO)-based optical parametric amplifier (OPA) takes place in a $AgGaS_2$ crystal and yields pulses that are ~60 fs in duration and centered at 5.1 μm (1960 cm^{-1}). A 7% portion of each pulse is split off to generate a probe beam, while the remaining beam intensity enters a Ge AOM-based pulse shaper. Before entering the shaper, the remaining 90% portion of the pulse is split in half to generate portions that will comprise the vertical and horizontal components of the polarization-tailored beam. Both portions of the pulse are frequency dispersed by a 100 g mm^{-1} grating with different angles of incidence and focused by an f = 12.5 cm cylindrical mirror before being subjected to a phase-tailored mask. The frequency elements of the two separate portions of the pulse are collimated by a second cylindrical mirror before recombination by a second grating. The two pulses exit the shaper at different diffraction angles. One of the two pulses is rotated by a $\lambda/2$ waveplate and sent through a delay line in order to account for path differences of the two pulses. The pulses, now bearing polarizations perpendicular to one another are temporally and spatially recombined at a wire grid polarizer. This allows for the generation of two phase-shaped mid-IR pulses with polarizations

perpendicular to one another. These two pulses are combined at a wire grid polarizer, yielding an ~1 μJ programmable pulse with a bandwidth of ~200 cm^{-1}. The resultant pulse becomes the pump pulse in our pump–probe experiments.

2.2. Optimizing vibrational ratios with a genetic learning algorithm

Experiments were conducted in which the ratios of the intensities of the A_1 bleach ($0 \rightarrow 1$ transition) and E bleach were optimized relative to one another. These ratios were used as fitness values in an evolutionary algorithm [13]. Individuals consisted of two sets of 12 parameters that defined a unique electric field generated from a sum of four sine waves,

$$\varphi(\omega)=\sum_{i=1}^{4} a_i \sin(b_i\omega+c_i), \tag{1}$$

in which one set of parameters modulated the phase of the vertical components of the electric field and the second set modulated the horizontal components. A sum of sine waves was used to approximate a Fourier series and sample a large portion of the available configuration space with a minimal number of variable parameters. Sinusoidal phase modulation in coherent control experiments has been previously employed by our group [25] and others [34,35]. Populations consisted of 40 individuals. The three most fit individuals from each population were incorporated, unchanged, into the next population, while the remaining individuals underwent crossing and random point mutation. New populations were generated until the algorithm converged at an electric field that best optimized the desired intensity ratio. In those experiments in which only phase shaping and not polarization shaping was used to optimize an intensity ratio, the same mask was used for both the vertical and horizontal components of the electric fields. We have demonstrated in our initial report describing our pulse shaper that equivalent phase masks yield linearly polarized pulses with $\theta = 45°$ relative to the probe pulse [30].

2.3. Pulse characterization

The intensity of each optimized pulse as a function of time was measured by using a linear, polarization sensitive cross correlator (figure 1). Our method is similar to time-resolved ellipsometry methods reported previously [9,36]. The fidelity of the polarization was checked at the sample using wire grid polarizers. There is less than a 5° relative rotation of the horizontal and vertical fields due to optics after the cross-correlator. We experimentally characterize the pulses even though they can be calculated from the AOM waveform as a check of their accuracy since the design of the shaper reduces the mask resolution by half (to about 100 resolvable frequency elements). A portion of the probe beam served as the gating pulse and was spatially overlapped with the shaped pulse using a 50/50 beam splitter. The gate pulse was scanned in time with a mechanical delay stage and fluctuations in intensity were monitored with a single channel MCT detector. The electric field is depicted in three dimensions by measuring two separate linear cross-correlations in which the gate pulse that is being interfered with the tailored pulse is oriented both parallel and perpendicular to the optimized pulse using a λ/2 waveplate. A vector sum of the two cross correlations yields the 3D electric field. The gate pulse was found to have an ~60 fs duration using a 2nd order auto-correlator. A MOSAIC algorithm was subsequently applied to ensure that the contributions of higher-order phase distortions were negligible [24,37]. The interferometric stability of our setup was λ/10 over the course of our measurements, which affects the phase of our cross correlations very little [30]. This assertion was verified for the experiments reported here by monitoring the temporal fringes in a cross-correlation.

3. Results

3.1. Transform-limited pulses

Shown in figures 2(a) and (b) is the transient absorption spectrum of $Mn(CO)_5Br$ measured with a single transform-limited pump pulse followed 2 ps later by a transform-limited probe pulse. The negative peak at 2052 cm^{-1} (peak (i)) corresponds to the fundamental transition of the *E* mode, while the positive going feature at 2039 cm^{-1} (peak (ii)) arises due to the sequence transition, $\upsilon = 1–2$. Similarly, the weaker positive and negative features at 2002 cm^{-1} (peak (iii)) and 1979 cm^{-1} (peak (iv)) arise due to fundamental and sequence transitions of the A_1 mode. The separation between (i) and (ii) (Δ_E = 13 $cm^{-}1$) is primarily the diagonal anharmonicity of the *E* stretch, while the separation of (iii) and (iv) (Δ_{A_1} = 23 cm^{-1}) is due to the anharmonicity of the A_1 stretch. To investigate the origin of these modes, we also collected 2D IR spectra with parallel polarized pump and probe beams as well as perpendicular polarizations, as shown in figure 3. Negative going features due to the fundamental transitions of the A_1 and *E* modes appearing on the diagonal, which correspond to features (i) and (iii) in the transient absorption spectra. The sequence bands for both of these features (ii and iv) appear as shifted to lower energy along the ω_{probe} axis due to the anharmonicity of these vibrations. Weak off-diagonal cross peaks due to coupling between the A_1 and *E* modes appear in the upper left- and lower right-hand corners of the parallel and perpendicular spectra. These features are stronger in the perpendicular spectra, indicating that the transition dipoles of the A_1 and *E* modes are oriented in very different directions if not orthogonally to one another. The off-diagonal anharmonicity (Δ_{E+A_1}) of these cross peaks is 5 cm^{-1}. The energy levels that give rise to the features in the transient and 2D spectra are diagrammed in figure 2(c). The fact that such weak cross peaks are observed, indicates that the coupling between the carbonyl local modes is much bigger than the local mode anharmonicity (~30 cm^{-1} compared with other metal carbonyl systems), so that the vibrational Hamiltonian of $Mn(CO)_5Br$ is nearly diagonal in the normal mode basis set. The spectra shown here represent the starting point from which we will shape the phase, amplitude and polarization of the pump beam to affect the relative populations of these states.

3.2. Optimizations and electric field characterization

Experiments were conducted in which electric fields were generated to optimize the intensity of the A_1 fundamental relative to the *E* fundamental (i.e. the A_1/E ratio). The resultant pump–probe spectrum is plotted in figure 2(a) along with the pump–probe spectrum generated with a transform limited pulse. Improvement factors were calculated by normalizing to the optimized peak and measuring the difference between the minimized peak for the transform limited and optimized pulses. An improvement factor of 3.0 relative to the transform limited pulse was achieved for this optimization. Similarly, the *E* fundamental intensity was optimized relative to that of the A_1 mode (E/A_1 ratio), and an improvement factor of 2.3 was achieved, as shown in figure 2(b). In figures 2(a) and (b), the pump–probe spectra are normalized to the optimized feature (peak c in figure 2(a) and peak a in figure 2(b)).

The electric fields to which the evolutionary algorithm converged are plotted in figure 4. Both optimized pulses exhibit a shift in polarization approximately half-way through the duration of the pulse. In the case of the pulse generated to optimize A_1/E, a polarization shift from 26° to 74° takes place at −0.5 ps, whereas in the case of the E/A_1 optimization, a polarization shift from 71° to 21° takes place at 0 ps. These polarization shifts are nearly mirror images of one another and may qualitatively suggest a shared mechanism for optimization. Running Fourier transforms track the frequency information as a function of time and were calculated for each of the four cross correlations used to generate the 3D electric fields (figure 5). A 70 fs Gaussian window was scanned over each of the cross-correlations and Fourier transformed. It is evident from the running Fourier transforms that variations in intensity at the A_1 and *E* transitions are

not responsible for suppressing the corresponding pump–probe features of these modes. Such intensity fluctuations are obviated by the lack of amplitude tailoring in our investigations.

3.3. Comparison to phase-only shaping

In order to ensure that polarization control was in fact improving our capacity to optimize the A_1/E and E/A_1 mode intensity ratios, we conducted comparative optimizations in which only phase shaping was employed. The same experimental conditions and the same upper and lower bounds on the phase parameters (a_i, b_i, and c_i in equation (1)) were employed for both sets of optimizations; however, while separate phase masks were generated for the vertical and horizontal components of the electric fields in the polarization-shaping scenario, the same mask was used for both components in the phase-only-shaping scenario. Hence, the linearly polarized pulse was allowed to sample the same configuration space as either the horizontal or vertical component of the polarization-shaped pulse. In both cases, the maximum-allowed vector components in the vertical and horizontal directions are the same. Improvements of the fitness values as a function of generation are plotted in figure 6 for optimizations of the A_1/E and E/A_1 intensity ratios given both polarization shaping and phase-only shaping. In the case of the A_1/E optimization, polarization shaping offers an increase in fitness improvement by a factor of 1.5 over phase-only shaping, whereas for the E/A_1 optimization, polarization shaping offers a factor of 2.3 increase in fitness improvement over phase-only shaping. The 45° angle of the pump relative to the probe pulse polarization does not influence the results because we are comparing the relative populations of the A_1 and E modes. Hence, in enhancing vibrational modes, polarization shaping offers a clear improvement over phase shaping alone, by 150–230%. Thus, polarization shaping is a useful tool in mid-IR coherent control experiments in analogy to previous work in the visible and near-IR regions [32, 33].

4. Discussion

As we have experimentally demonstrated, polarization shaping can enhance the selectivity of IR transitions as compared with the selectivity afforded solely by phase shaping. Since the model compound studied here has two well-resolved frequency transitions, one transition could have been selected over the other by amplitude shaping or by filtering the spectrum of the pump pulse, as is often done to collect 2D IR spectra [38]. The aim of this paper is to explore whether the electric field direction can be employed as well, which may be useful in discriminating between transition dipoles with degenerate energies, but different directions. Toward this aim, we present in this section a formalism by which polarization shaping can be treated separately from amplitude shaping or phase shaping. Using this formalism, we discuss possible mechanisms by which polarization shaping should be able to enhance or suppress transitions by changing the probability that the IR electric fields interact with molecular transition dipoles.

In an isotropic sample, the probability that an electric field linearly polarized along the *z*-axis will interact twice with a single transition dipole is given by

$$\langle ZZ\rangle = \frac{1}{4\pi}\int_0^{2\pi} d\varphi \int_0^{\pi} \sin\theta \cos^2\theta d\theta = \frac{1}{3}, \tag{2}$$

where φ and θ are the azimuth and elevation angles, respectively, that define the position of the transition dipole. The projections of the pulses onto the dipole are integrated over all space in order to obtain the probability that the pulses interact with the transition dipole. The rotational motion of the molecule between the two pulse interactions is neglected. In a perturbative description of the light–matter interaction between the laser fields and the molecules, equation (2) represents the orientational part of the two-point correlation function used to describe linear

spectroscopies $\langle Z\,Z\rangle = \langle \mu \cdot Z \mu \cdot Z\rangle$, where μ is the transition dipole and Z is in the laboratory molecular frame. This term only includes the projection of the pulse and emitted electric fields (e.g. $u \cdot z$) and not the electric field strength or the shape of its envelopes [39]. The strength and shape of the envelopes are included by convoluting with the molecular response term, which is not written here. Separability of the orientational and molecular responses is only possible when the rotational motions are independent of the remaining degrees of freedom, which is a good approximation for most molecules [40]. This description of the sample macroscopic polarizability is useful, because it allows the signal strength from the pulse polarizations to be computed separately from their amplitudes or phases in the limit such that the ordering of the field–matter interactions does not change. Polarization shaping can be thought of as amplitude shaping in a rotating frame, but then separability cannot be used to simplify the calculation of the signal and a convolution of the full electric field shape with the molecular response is required.

According to equation (1), 33% of the molecules contribute to the measured signal in an absorption experiment with a single laser pulse. In a 3rd-order nonlinear absorption experiment, like pump–probe spectroscopy, there are two interactions with the pump and two with the probe electric fields. Thus, the orientational description becomes [41]

$$\langle ZZZZ\rangle = \frac{1}{4\pi}\int_0^{2\pi} \mathrm{d}\varphi \int_0^{\pi} \sin\theta \cos^4\theta \mathrm{d}\theta = \frac{1}{5}, \tag{3}$$

for pump and probe with equal linear polarizations that all interact with the same transition dipole. For pump and probe pulses orthogonally polarized, the orientational description is

$$\langle XXZZ\rangle = \frac{1}{4\pi}\int_0^{2\pi} \cos^2\varphi \mathrm{d}\varphi \int_0^{\pi} \sin^3\theta \cos^2\theta \mathrm{d}\theta = \frac{1}{15}. \tag{4}$$

Hence, if the polarization of the pump pulse is rotated by 90°, the signal intensity will decrease by a factor of 3 for a molecule with a single transition dipole.

Equations (2) and (3) provide the simplest means by which a polarization-shaped pump pulse could be used to selectively alter the observed absorbance of one vibrational mode over another. If a polarization-shaped pump pulse like that shown in figure 7 was created in which half of the pulse was resonant with one transition and half with the other and if the two halves were orthogonally polarized, then one transition could be suppressed over the other by choosing the resonant field that was aligned with the probe pulse. For example, if it was desired that the A_1 mode be enhanced over the E modes, then a shaped pulse, in which the frequency components on-resonance with the A_1 mode are given the same Z -polarization as the probe pulse, would yield a signal measured from that portion of the shaped pump pulse which scales as $\langle Z\,Z\,Z\,Z\rangle$. If the frequency components from that same pulse on-resonance with the E modes had X-polarization, then the signal measured from that portion of the shaped pump pulse would scale as $\langle X\,X\,Z\,Z\rangle$, and would be three times weaker.

The above argument assumes that the interaction of the electric fields with the molecule is only due to the transition dipole contribution to the interaction energy and is also based on a perturbative description of the field–matter interaction. Higher terms in the expansion of the interaction energy, such as multipole and circular dichroism terms, could contribute to selectivity as well, but their effects are presumably small compared to the dipolar terms. The circular dichroism term in the expansion of the interaction energy is as much as 10000 times

smaller than the dipole terms, for example [42]. As for the perturbative description of the light–matter interaction, sequence bands up to $\upsilon = 6$–7 are often observed in the transient absorption spectra of metal carbonyl compounds, especially when using shaped or chirped mid-IR pump pulses [25]–[27]. Thus, it would not be unexpected to have processes up to 13th order to be involved. With intense and shaped pulses, it is more accurate to understand the light–matter interaction by explicitly solving the time-dependent Schrödinger equation [43,44].

In the current experiments, we believe that the polarization-shaped pump pulses are causing predominately lower-order processes, because the transient absorption spectra do not exhibit sequence bands beyond transitions involving $\upsilon = 1$–2. However, we note that the higher-order processes can be used to optimize the population of low vibrational states, such as $\upsilon = 2$, without significantly populating higher quantum states [25]. Higher-order processes should also give rise to better vibrational selectivity through polarization shaping, as we now elucidate. Consider the orientation terms for a 5th-order process involving a single transition dipole [45]–[47]:

$$\langle ZZZZZZ\rangle = \frac{1}{4\pi}\int_0^{2\pi} \mathrm{d}\varphi \int_0^{\pi} \sin\theta \cos^6\theta \mathrm{d}\theta = \frac{1}{7} \tag{5}$$

and

$$\langle XXZZZZ\rangle = \frac{1}{4\pi}\int_0^{2\pi} \cos^2\varphi \mathrm{d}\varphi \int_0^{\pi} \sin^3\theta \cos^4\theta \mathrm{d}\theta = \frac{1}{35}. \tag{6}$$

Thus, there is a factor of 5 reduction in signal intensity for a 5th-order process, compared with a factor of 3 for a 3rd-order process. Therefore, if a polarization-shaped pump pulse like that shown in figure 7 was created, only with each half of the pulse interacting four times, rather than twice, then one mode could be reduced in intensity compared with the other by 80% (compared with 66% for a 3rd-order process). 7th and higher-order interactions would lead to a further suppression. Thus, from our experiments and this simple perturbative description of the field–matter interaction, we believe that it is straightforward to achieve mode selectivity.

Transient absorption spectroscopy is not the best probe for understanding the mechanism by which the shaped pump causes mode selectivity, because it is difficult with transient absorption spectroscopy to resolve the contributions of sequence bands. Except in molecules where the local mode anharmonicity is comparable with the coupling strengths, the energy difference of the $\upsilon = 0$ to 1 transitions is nearly degenerate with the energy difference between the $\upsilon = 1$ states and the combination band [3,48]. Thus, in transient absorption spectra, the contributions from the sequence bands cannot typically be resolved from the fundamentals. In this regard, 2D IR spectroscopy is a much better probe. With a 2D IR probe, the sequence bands create cross peaks in the spectra while the fundamental transitions lie on the diagonal, and thus are resolved from one another. In the present study, we have not used 2D IR spectroscopy to probe the effects of the shaped pulses. In the $Mn(CO)_5Br$ system, it is unlikely that the combination bands are playing a significant role in the transient absorption spectra because the off-diagonal anharmonicity in this system is so small, which is why the cross peaks in the 2D IR spectra are weak. Thus, in this case, we believe that the mechanism for mode selectivity with polarization shaping is independent of the coupling Hamiltonian. Further experiments are necessary to definitively verify this hypothesis.

5. Conclusions

We have demonstrated a capacity to control the intensities of the A_1 and E modes of $Mn(CO)_5Br$ using polarization-tailored mid-IR pulses. We further demonstrate that our ability to optimize the ratios of the two modes in question is enhanced with polarization control as opposed to phase-only tailoring. A genetic algorithm was used to find the optimized pulse shape, but if the transition dipole directions, vibrational eigenvalues and transition dipole strengths are known, then the time-dependent Schrödinger equation can be directly solved and used as a basis to guide the search for properly shaped pulses [43,44]. Moreover, since transition dipoles are a good approximation for vibrational modes and molecular rotation is slow compared with vibrational relaxation in condensed phase systems, it should also be possible to theoretically search for pulse shapes by simply minimizing or interfering the appropriate orientational tensor elements [41,45] for the desired Feynman pathway following the formalism outlined in the Discussion section. Thus, one should be able to predictively design polarization-shaped pulses to optimize signals in 2D IR spectra, for example. In the model system studied here, which had two spectrally resolved vibrational modes, amplitude shaping could have been used to selectively excite one mode over the other. We expect that polarization shaping will find use in discriminating between degenerate modes that have different transition dipole directions, such as the amide I normal modes of peptides and protein secondary structures. We also note that methods like those discussed here are not limited to vibrational spectroscopy, but can also be applied to visible chromophores as well [49], such as the Fenna–Matthews–Olson light harvesting complex from green photosynthetic bacteria, which can also be described by a simple excitonic Hamiltonian and studied with polarization sensitive 2D visible spectroscopies [50].

Acknowledgments

This research was funded by the Packard Foundation and the National Institutes of Health (DK79895).

References

1. Krummel AT, Mukherjee P, Zanni MT. J Phys Chem B 2003;107:9165.
2. Woutersen S, Hamm P. J Phys Chem B 2000;104:11316.
3. Zanni MT, Gnanakaran S, Stenger J, Hochstrasser RM. J Phys Chem B 2001;105:6520.
4. Zanni MT, Ge NH, Kim YS, Hochstrasser RM. Proc Natl Acad Sci USA 2001;98:11265. [PubMed: 11562493]
5. Xiong W, Zanni MT. Opt Lett 2008;33:1371. [PubMed: 18552963]
6. Ding F, Zanni MT. Chem Phys 2007;341:95.
7. Garrett-Roe S, Hamm P. J Chem Phys 2009;130:164510. [PubMed: 19405597]
8. Brixner T, Gerber G. Opt Lett 2001;26:557. [PubMed: 18040384]
9. Plewicki M, Weise F, Weber SM, Lindinger A. Appl Opt 2006;45:8354. [PubMed: 17068582]
10. Ninck M, Galler A, Feurer T, Brixner T. Opt Lett 2007;32:3379. [PubMed: 18059939]
11. Plewicki M, Weber SM, Weise F, Lindinger A. Appl Phys B 2007;86:259.
12. Polachek L, Oron D, Silberberg Y. Opt Lett 2006;31:631. [PubMed: 16570421]
13. Judson RS, Rabitz H. Phys Rev Lett 1992;68:1500. [PubMed: 10045147]
14. Assion A, et al. Science 1998;282:919. [PubMed: 9794756]
15. Levis RJ, Menkir GM, Rabitz H. Science 2001;292:709. [PubMed: 11283357]
16. Daniel C, et al. Science 2003;299:536. [PubMed: 12543966]
17. Herek JL, et al. Nature 2002;417:533. [PubMed: 12037563]
18. Brixner T, Damrauer NH, Niklaus P, Gerber G. Nature 2001;414:57. [PubMed: 11689940]
19. Bartels RA, et al. Phys Rev A 2004;70:043404.
20. Demirplak M, Rice SA. J Chem Phys 2002;116:8028.

21. Dela Cruz JM, et al. J Phys Chem A 2004;108:53.
22. Lozovoy VV, Dantus M. Chem Phys Chem 2005;6:1970. [PubMed: 16208734]
23. Shim SH, Strasfeld DB, Fulmer EC, Zanni MT. Opt Lett 2006;31:838. [PubMed: 16544641]
24. Shim SH, Strasfeld DB, Zanni MT. Opt Express 2006;14:13120. [PubMed: 19532209]
25. Strasfeld DB, Shim SH, Zanni MT. Phys Rev Lett 2007;99:038102. [PubMed: 17678332]
26. Strasfeld DB, Shim SH, Zanni MT. Adv Chem Phys 2009;141:1.
27. Ventalon C, et al. Proc Natl Acad Sci USA 2004;101:13216. [PubMed: 15319472]
28. Oron D, Dudovich N, Yelin D, Silberberg Y. Phys Rev A 2002;65:043408.
29. Hauer J, Skenderovic H, Kompa KL, Motzkus M. Chem Phys Lett 2006;421:523.
30. Middleton CT, Strasfeld DB, Zanni MT. Opt Express 2009;17:14526. [PubMed: 19687931]
31. Voronine D, Abramavicius D, Mukamel S. J Chem Phys 2006;124:034104. [PubMed: 16438564]
32. Brixner T, et al. Phys Rev Lett 2004;92:208301. [PubMed: 15169385]
33. Weise F, Weber SM, Plewicki M, Lindinger A. Chem Phys 2007;332:313.
34. Meshulach D, Silberberg Y. Nature 1998;396:239.
35. Wollenhaupt M, et al. Phys Rev A 2006;73:063409.
36. Jellison GE, Lowndes DH. Appl Phys Lett 1985;47:718.
37. Bender DA, Hasselbeck MP, Sheik-Bahae M. Opt Lett 2006;31:122. [PubMed: 16419898]
38. Shim SH, Strasfeld DB, Ling YL, Zanni MT. Proc Natl Acad Sci USA 2007;104:14197. [PubMed: 17502604]
39. Mukamel, S. Nonlinear Spectroscopy. New York: Oxford University Press; 1995.
40. Laage D, Hynes JT. Science 2006;311:832. [PubMed: 16439623]
41. Hochstrasser RM. Chem Phys 2001;266:273.
42. Johnson WC. Annu Rev Biophys Biophys Chem 1988;17:145. [PubMed: 3293583]
43. Meier C, Heitz MC. J Chem Phys 2005;123:161–72.
44. Gollub C, Korff BMR, Kompa KL, de Vivie-Riedle R. Phys Chem Chem Phys 2007;9:369. [PubMed: 17199153]
45. Ding F, Fulmer EC, Zanni MT. J Chem Phys 2005;123:094502.
46. Bredenbeck J, Helbing J, Hamm P. J Chem Phys 2004;121:5943. [PubMed: 15367023]
47. Tokmakoff A. J Chem Phys 1996;105:13.
48. Fulmer EC, Mukherjee P, Krummel AT, Zanni MT. J Chem Phys 2004;120:8067. [PubMed: 15267726]
49. Cao JS. J Lumin 2000:87–930.
50. Read EL, et al. Proc Natl Acad Sci USA 2007;104:14203. [PubMed: 17548830]

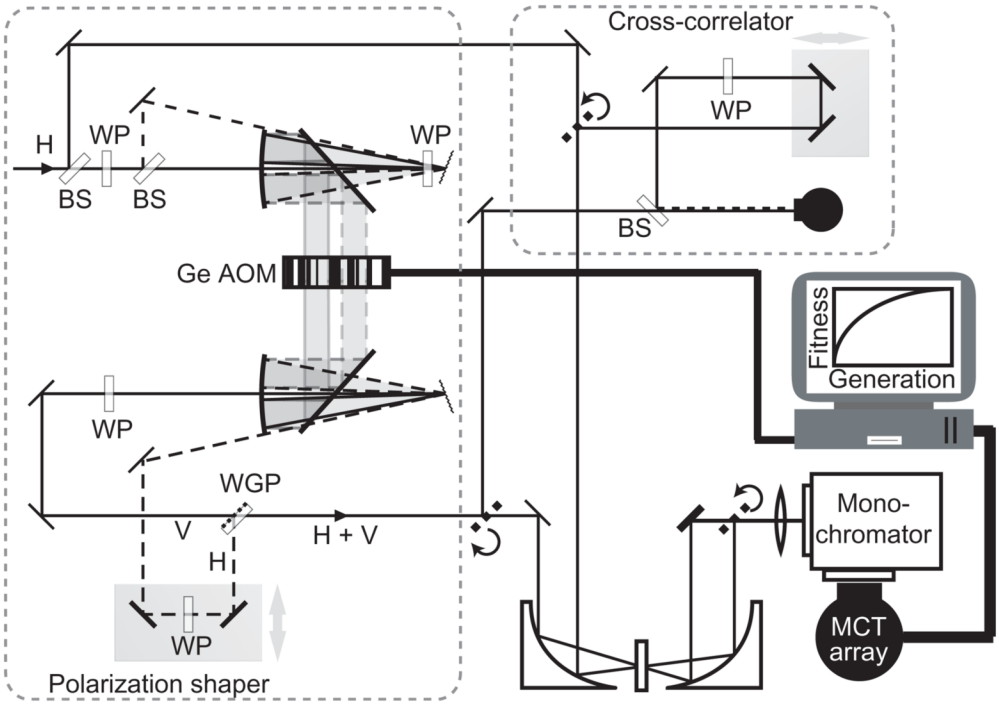

Figure 1.
Schematic of the polarization-shaped pump–probe layout. WP, waveplate; BS, beamsplitter; WGP, wire grid polarizer; G, grating; H, horizontal and V, vertical.

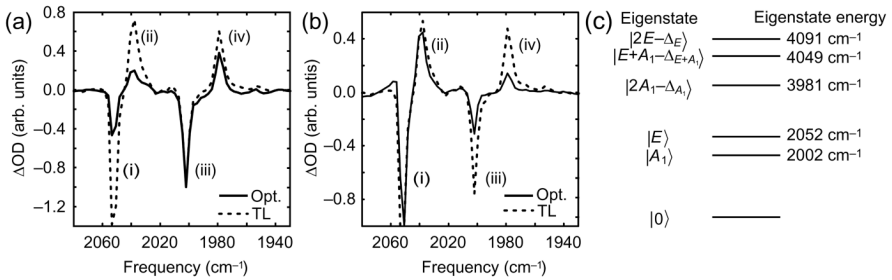

Figure 2.

Experimental pump–probe spectra in which the A_1/E fundamental intensity ratio was optimized (a), and the E/A_1 fundamental intensity ratio was optimized (b). Peak (i) is the E (0–1) transition, peak (ii) is the E (1–2) transition, peak (iii) is the A_1 (0–1) transition and peak (iv) is the A_1 (1–2) transition. The dashed line is the pump–probe spectrum achieved with a TL pulse and taken immediately after each optimization. The spectra in (a) are normalized to the A_1 fundamental. The spectra in (b) are normalized to the E fundamental. An energy-level diagram corresponding to the fundamental and sequence transitions is depicted in (c).

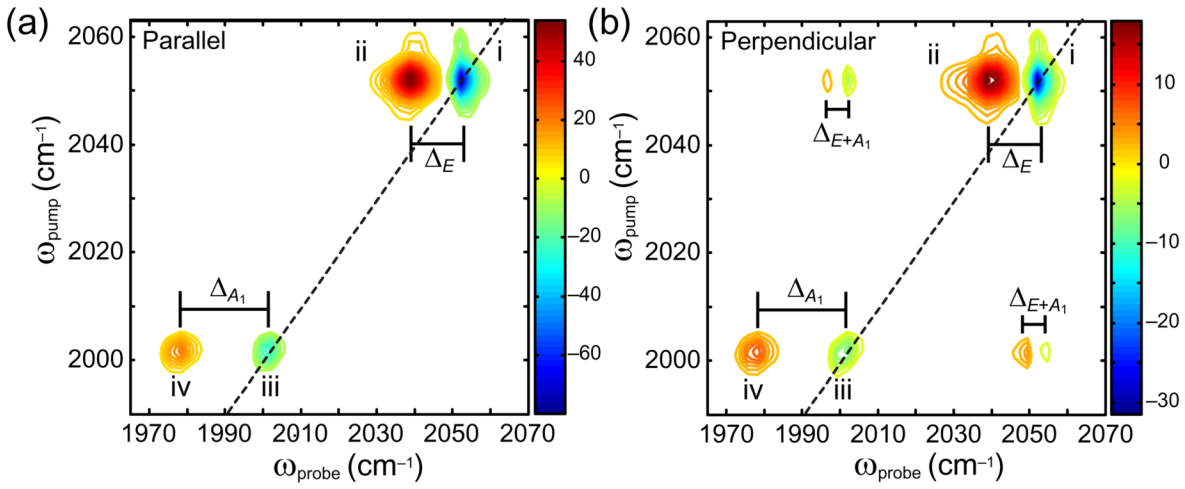

Figure 3.
2D IR spectra of $Mn(CO)_5Br$ taken with parallel (a) and perpendicular (b) beam polarizations. The anharmonic shifts for each fundamental and overtone pair are labeled.

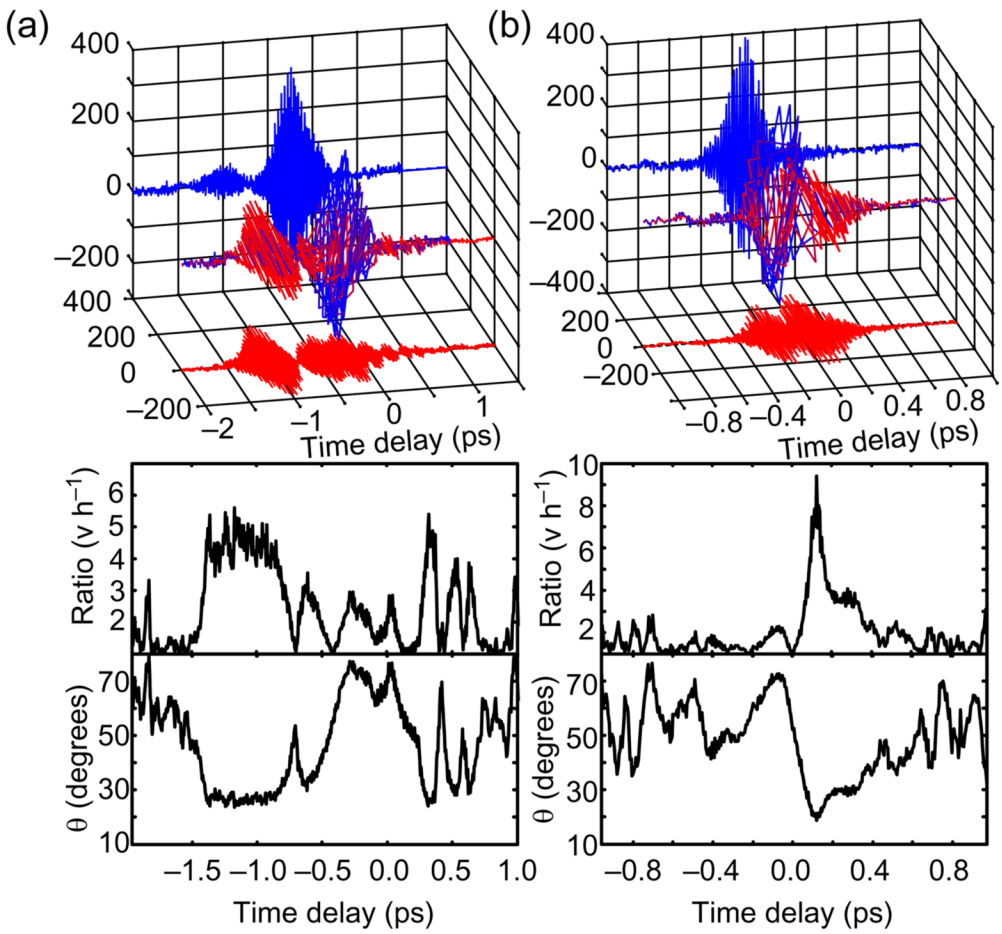

Figure 4.
Characterized electric fields for the optimized pulses. (Top) 3D representations of the optimized pulses, (mid) axis ratios and (bottom) polarizations as a function of time are plotted for the A_1/E (a) and E/A_1 (b) optimizations.

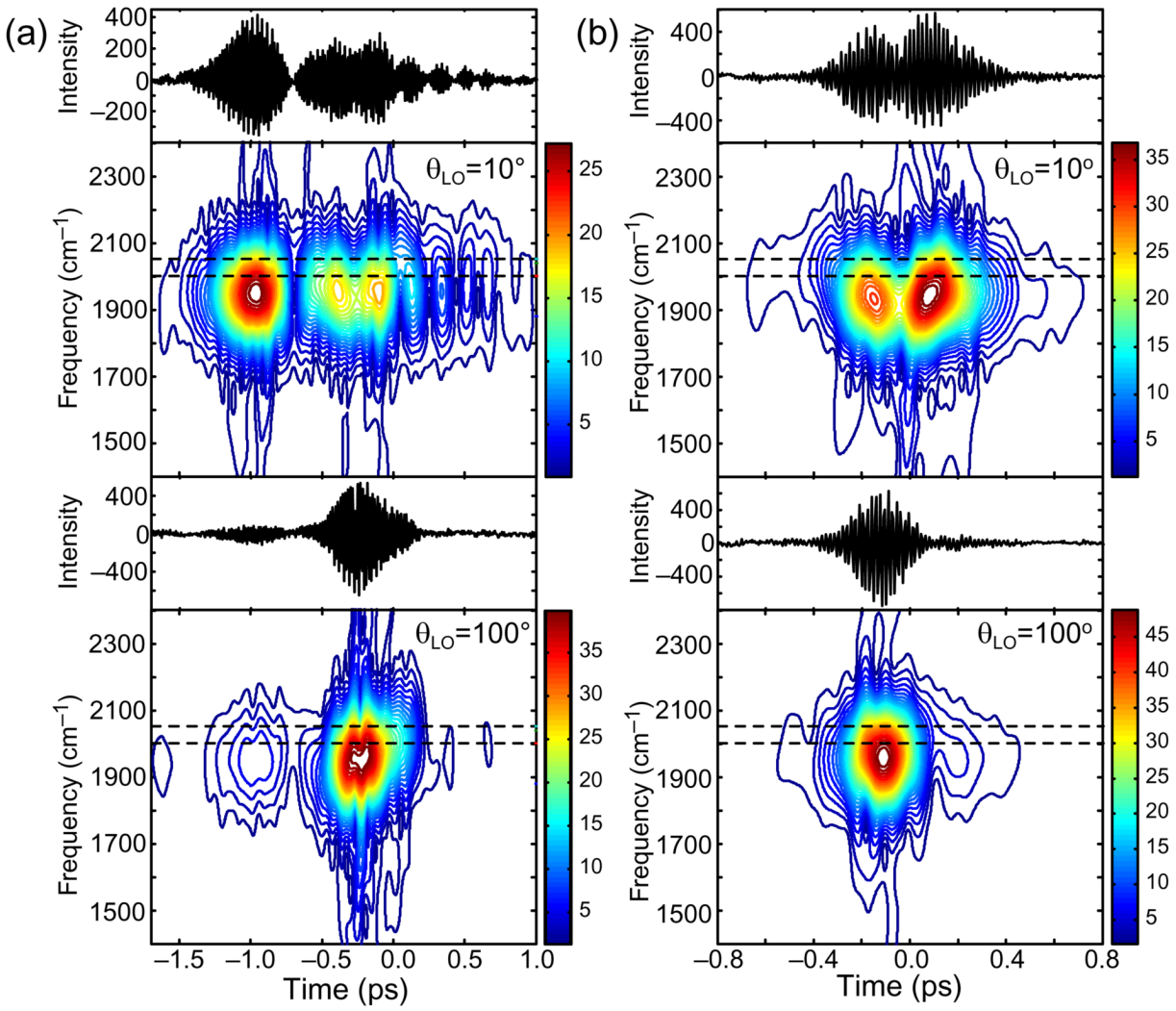

Figure 5.

Running Fourier transforms of the linear cross-correlations taken with θ_{LO} = 10° and θ_{LO} = 100° for the pulses optimizing the A_1/E fundamental ratio (a) and the E/A_1 fundamental ratio (b). The dashed lines at 2002 and 2052 cm^{-1} indicate the positions of the A_1 and E transitions, respectively.

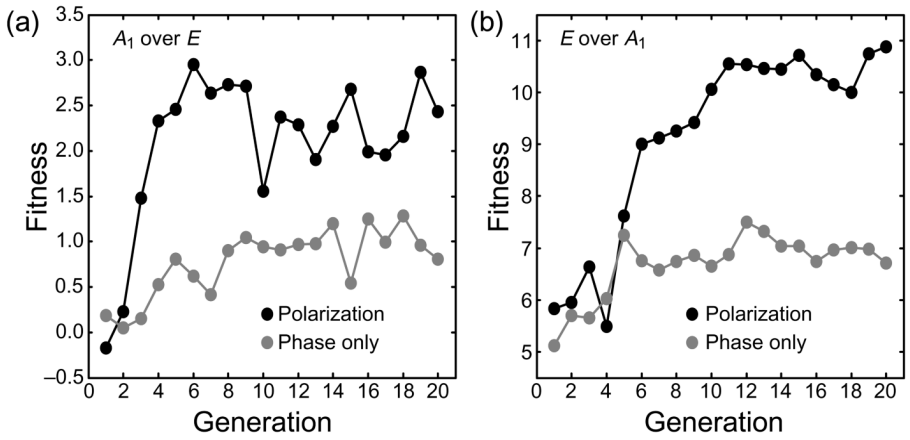

Figure 6.
Comparisons of the fitness curves for polarization shaping and phase-only shaping. The most fit individuals from each generation are plotted for the A_1/E (a) and E/A_1 (b) optimizations.

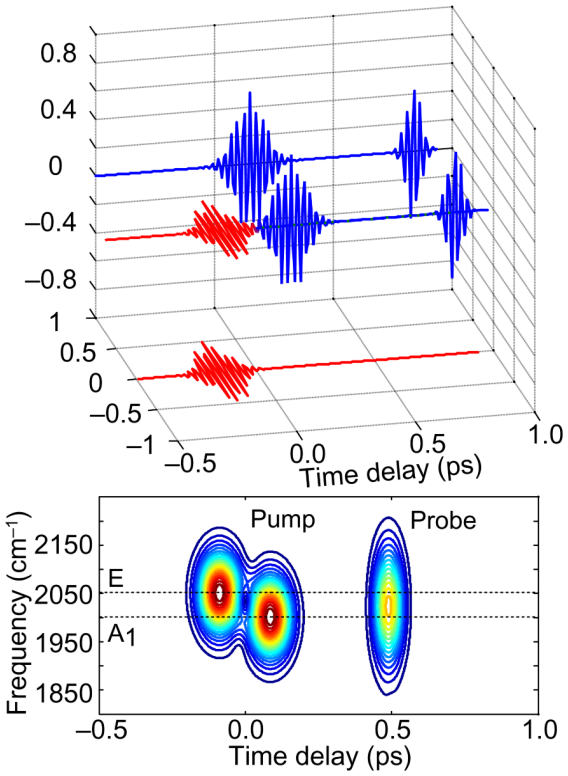

Figure 7.
Schematic of an electric field that will optimize the A_1 mode relative to the E mode based on the orientational effects described in section 4.